MADRID
inter.noise 2019
June 16 - 19
NOISE CONTROL FOR A BETTER ENVIRONMENT

Rolling noise in road and rail transportation systems

Lopez Arteaga, Ines[1]
Eindhoven University of Technology, Department of Mechanical Engineering, Eindhoven, The Netherlands
KTH Royal Institute of Technology, Marcus Wallenberg Laboratory for Sound and Vibration Research, Stockholm, Sweden

ABSTRACT

Long term exposure to ground transportation (road and rail traffic) noise is, after air pollution, the main environment-related health stressor in densely populated areas and compromises the quality of life and, indirectly, the life expectations of millions of people. The main source of ground transportation noise at speeds up to 130 km/h in road traffic and up to 300 km/h in rail traffic is rolling noise; noise generated due to the interaction between tyre and road (respectively wheel and rail). Although at first sight noise generation in these two transportation systems might seem unrelated, exploring the common aspects provides valuable insight in current practices for the modeling, prediction and abatement of rolling noise. In this paper the sound and vibration generation mechanisms due to tyre/road and wheel/rail interaction are discussed, focusing on the similarities and differences between the sound and vibration generation mechanisms in these two systems. This perspective is further extended to the discussion of modelling strategies and source characterization methods, with a particular emphasis on the influence of surface roughness on contact force generation. Finally, rolling noise source separation methods are touched upon, since they are a necesary tool to assess the impact of noise and vibration mitigation measures in both road and rail traffic systems.

Keywords: tyre/road noise, wheel/rail noise, contact forces, roughness, source separation
I-INCE Classification of Subject Number: 30
(see http://i-ince.org/files/data/classification.pdf)

1. INTRODUCTION

Ground transportation noise is becoming an increasingly big problem in densely populated areas. This noise consists mainly of road and rail transportation noise. For road transportation tyre/road noise is the dominating noise source for constant driving

[1] i.lopez@tue.nl/inesla@kth.se

speeds of 40 km/h and higher for combustion engines and for all urban speeds in the case of electric vehicles [1]. On the other hand for rail transportation, wheel/rail rolling noise is the main source of noise on open line [2].

Rolling noise of road and rail vehicles is very similar in nature, since both originate in vibrations caused by roughness-induced dynamic contact forces. In this paper the sound and vibration generation mechanisms due to tyre/road and wheel/rail interaction are discussed, focusing on the similarities and differences between the sound and vibration generation mechanisms in these two systems. In essence the source of noise are the dynamic contact forces caused by the (combined) surface roughness, as discussed in [3]. Here a brief summary of the contat force generation process is given. Finally rolling noise source separation methods are discussed.

2. FROM SURFACE ROUGHNESS TO SOUND GENERATION

2.1 Background

Ground transportation is based on rolling contacts due to their inherent low resistance to motion. However due to the surface roughness of the elements in contact, dynamic forces are generated during the rolling motion. These forces generate vibrations of the structures in contact and these vibrations lead to noise. The frequency of the excitation force is related to the wavelength of the surface roughness through the vehicle speed:

$$f = \frac{V}{\lambda}, \tag{1}$$

where f $[Hz]$ is the frequency, λ $[m]$ the wavelength and V $[m/s]$ the vehicle speed. This relationship is fundamental to understanding the dynamic response to rolling excitation and the negative effects associated to it as is schematically shown in Figure 1.

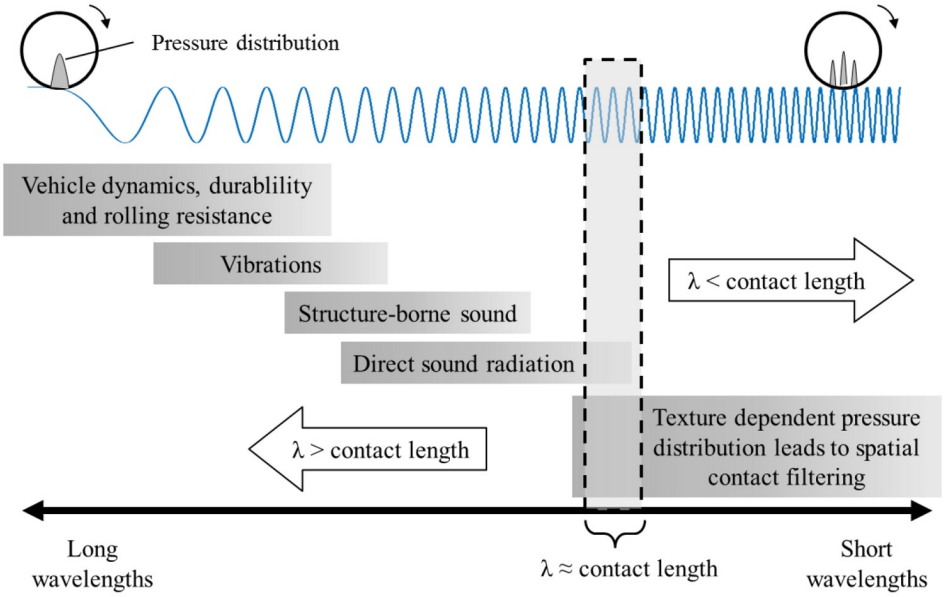

Figure 1: Relation between surface texture wavelength and vibroacoustic aspects caused by rolling excitation [4].

Very long wavelengths lead to low frequency excitation which, in case of coincidence with structural resonances, might lead to structural durability problems and high rolling

resistance in tyres. For shorter wavelengths, comfort-related aspects such as vibrational disturbance and structure borne sound problems may appear. Even shorter wavelengths are usually accompanied by direct sound radiation from the rolling object or the supporting structure. Although the basic mechanism of roughness-induced vibrations is the same for tyre/road and wheel/rail interaction, there are significant differences in the contact, dynamic response and sound radiation mechanisms that are discussed in the following subsections.

2.2 Particularities of wheel/rail noise

For rail vehicles the combined surface roughness of wheel and rail excites vibrations in both systems as shown in Figure 2.

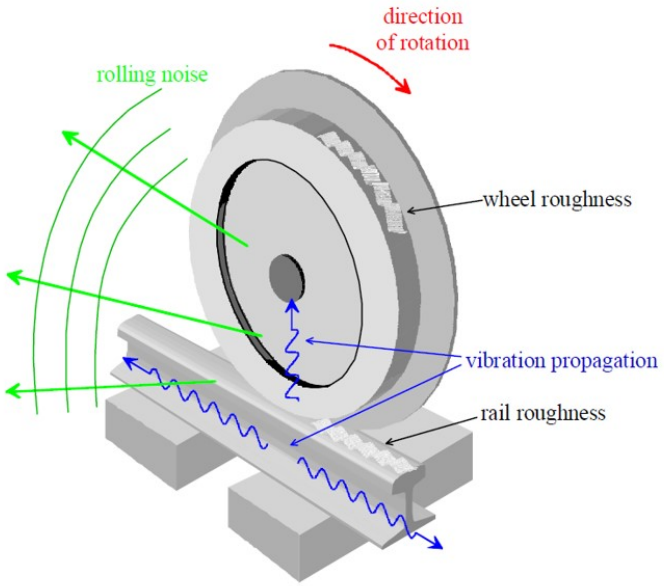

Figure 2: Wheel/rail noise generation [5].

Both wheel and rail are efficient sound radiators in a broad frequency range and therefore the roughness-induced vibrations lead partly to noise and are partly transmitted to the sleepers which in turn radiate sound as well. The vibration energy of the wheels is concentrated around the eigenmodes of the wheel, and dominates pass-by noise generally above 1500 Hz. The rail radiates broadband sound in the frequency region 250-1250 Hz, while the sleepers are the main contributors to the total pass-by noise at low frequencies, below about 400 Hz. The structural damping of railway wheels is very low, which means that all vibration modes excited will easily reach relatively large vibration amplitudes at their corresponding resonance frequencies and radiate sound efficiently, since the structural wavelengths are larger than the acoustic wavelengths for most frequencies of interest. On the other hand the track, unlike the road in tyre/road noise, is a major contributor to railway noise and the contact forces and the track response to these forces strongly depend on its dynamic properties, which are determined by: the rail properties, sleeper and rail pad properties and ballast properties. The fact that both track and vehicle actively contribute to the pass-by noise leads to the need of separating these contributions in order to be able to establish the noise levels originated by a certain vehicle (see Section 4).

2.3 Particularities of tyre/road noise

When a tyre rolls on a rough surface tyre vibrations are excited due to two main effects: the impacts caused by the tread blocks entering and exiting the contact area and the higher frequency excitation originated by the road roughness wavelengths of the order of the tread block size within the contact area. This is schematically illustrated in Figure 3(a)-(b). As the tread blocks travel along the contact length, they are compressed by the road roughness asperities and the generated forces are transmitted to the tyre belt (see Figure 3(b)). The contact forces cause the tyre to vibrate as shown in Figure 3(c). Unlike

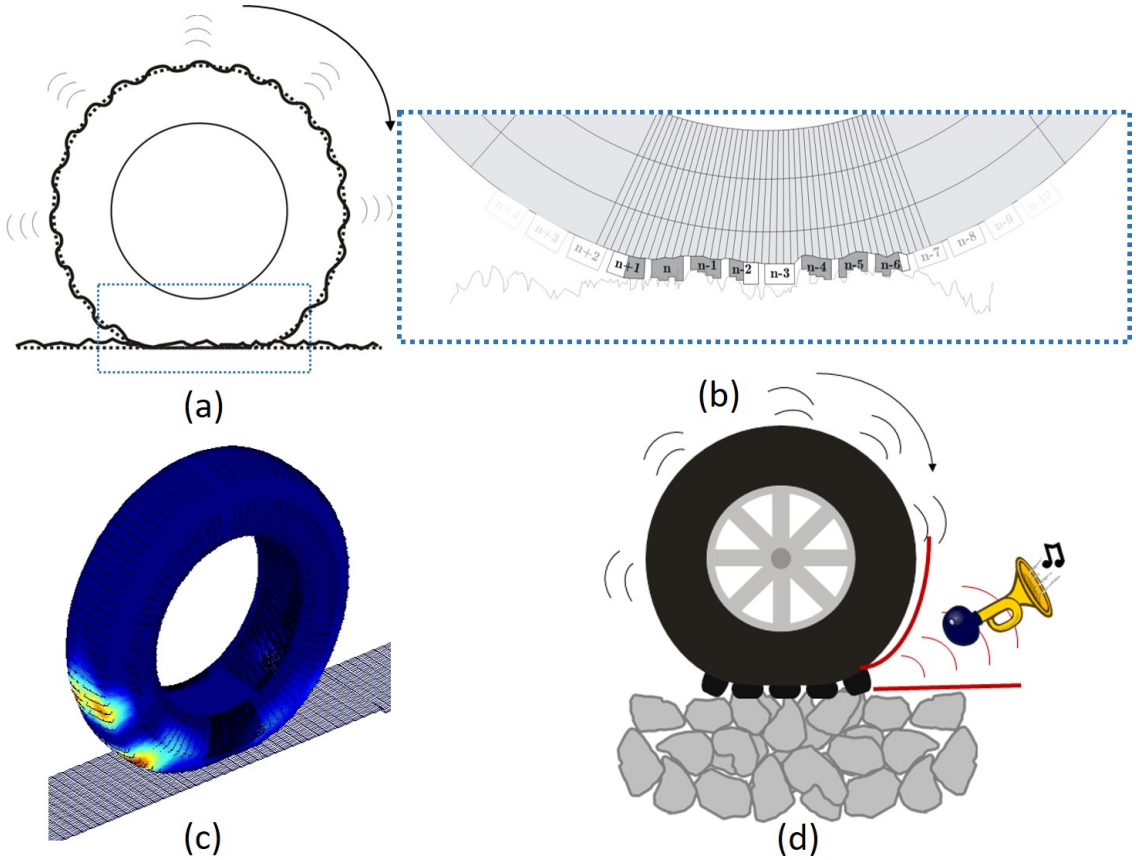

Figure 3: Overview of tyre/road sound generation: (a) Schematic view of tyre on rough road, (b) Detailed view of interaction between tread blocks and road surface asperities, (c) Tyre vibrations due to road roughness excitation, (d) Sound amplification through the horn effect.

vibrations in train wheels, elastic waves in tyres decay strongly as the distance to the contact area increases, which means that tyres themselves do not act as loudspeakers, as is the case for train wheels. In the case of tyre/road noise, the sound amplification is due to the horn effect as illustrated in Figure 3(d). The wedge at the leading edge of the tyre/road contact acts as a loudspeaker that can provide amplifications of the order of 30dB. Therefore road properties have a crucial influence on tyre/road noise. On the one hand road texture provides the excitation that makes the tyre vibrate and, on the other hand, a road with low acoustic absorption will greatly amplify the sound generated at the tyre/road contact. This inevitably leads to the conclusion that a smooth road with high sound absorption properties should greatly reduce tyre/road noise, as is the case [1]. One could argue that in the tyre/road interaction case the road is a "passive" contributor

to the generated sound, since it does not radiate sound itself (as the track does), but provides the absorption boundary conditions that regulate sound radiated by the tyres. As a consequence, establishing the relative contributions of tyre and road to the pass by noise is more straightforward than in the wheel/rail interaction case [1].

2.4 General modelling approach

The general modelling approach for vibro-acoustic predictions of wheel/track and tyre/road interaction is schematically given in Figure 4, where $\mathbf{f}(t,\Omega), \hat{\mathbf{f}}(\omega,\Omega)$ are the force vectors in time and frequency domain respectively, $\mathbf{G}(t,\Omega)$ is a matrix of Green's functions of the interacting subsystems, $\mathbf{Y}(\omega,\Omega)$ is the matrix of mobilities of the interacting subsystems, ω rad/s is the temporal frequency and Ω rad/s is the rotational velocity of the wheel/tyre. This approach has been exploited by several authors in both the road and railway noise communities, where some works include the influence of the rotational velocity on the system response (see for example [6], [7], [8], [9]) and others do not (see for example [10], [11]).

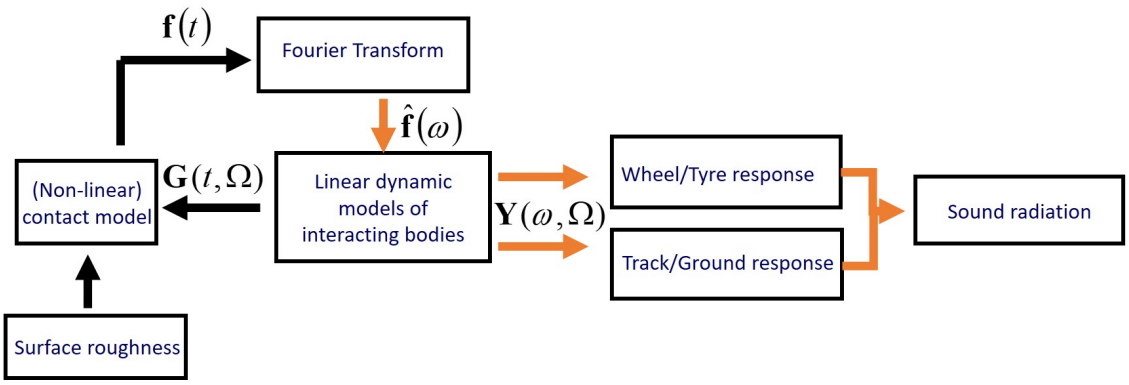

Figure 4: General modelling approach.

The idea behind the approach presented in Figure 4 is to separate the linear and nonlinear parts of the dynamic behavior of the system. For vibro-acoustic modelling it is reasonable to assume that the response of wheel/tyre and track/road is linear and can be described by Green's functions and mobilities. Which means that their response to the contact forces can be computed in the frequency domain. On the other hand, in order to account for the non-linear effects associated to the dynamic changes in the effective contact area caused by the surface roughness, the contact forces should be calculated in the time-domain. This leads to a two-step procedure where the contact forces are calculated in the time domain, considering the responses of the interacting structures through their Green's functions and with the (combined) roughness of the structures as input. In a second step, the contact forces are transformed to the frequency domain and the response of the interacting structures is obtained based on pre-calculated mobilities. This approach is computationally efficient, since the time consuming time-domain integration is performed with a relatively small model, including only the Green's functions for the parts of the structures that are potentially in contact.

Although this general approach is applied to both road and railway noise there are differences in how the interacting structures and the contact interaction are modelled and in the challenges involved. For wheel/track interaction wheel dynamics are modelled either as rigid body (when the track response is the main interest) or applying modal superposition of modes obtained from Finite Element (FE) models, which

is a straightforward procedure. Track dynamics are more complex to describe due to relatively large amount of parameters that influence the response of the track as mentioned in Section 2.2 (see [2]). The contact is often modelled as a point contact (see for example [12], [10]) applying Hertzian contact theory to determine the (nonlinear) contact stiffness and a filter to the combined roughness data in order to include the filtering effect of the contact patch (see [2]). This approach offers a limited description of the influence of the combined roughness on the contact forces as is further discussed in Section 3.

Regarding tyre/road interaction, the road is mostly modelled as an infinitely rigid surface and influences the sound generation through surface roughness and its sound absorption properties. Furthermore, tyres are complex structures, built of wires, cloth and several different rubber compounds, making accurate tyre modelling a hard task. A number of analytical models have been proposed in the literature such as plate models [13] and cylindrical shell models [14]. Although analytical models have proved to be valuable to study the general dynamic behavior of tyres, they are difficult to use in the tyre design process. On the other hand full FE models are too complex and time consuming. The alternative that has won in popularity in recent years is the Waveguide Finite Element Method (WFEM) [15], where the cross-section of the tyre is modelled using finite element (FE) and the vibration field in the circumferential direction is represented using waveguides. The second complexity factor in tyre/road noise is solving the contact problem between tyre and road. The size of the contact area depends on the load and the dynamic properties of the tyre and varies during rolling due to the road waviness and vehicle dynamics. Furthermore, the real contact area depends on the surface roughness of the road and is much smaller than the apparent contact area. Accurately predicting and measuring the 3-dimensional contact forces at the contact area is a challenging task that is further discussed in Section 4.

Summarizing, it is clear from the discussion in this and the previous section that a good understanding, accurate modelling and accurate measurements of rolling contact forces and the role of surface texture is key to the prediction and mitigation of transportation noise. Therefore in the following sections some detailed aspects of wheel/rail and tyre/road contact are discussed.

3. INFLUENCE OF SURFACE ROUGHNESS IN ROLLING CONTACTS

3.1 Modelling roughness-related nonlinearity in wheel/rail contact

Wheel/rail contact interaction is often simplified to a single contact point that moves along a line representing the combined wheel and rail roughness [2]. Assuming full compression of this combined roughness, Hertzian contact theory can be applied to derive the resulting contact force. The Hertzian contact stiffness is usually linearized around the equilibrium position corresponding to the static vehicle load and applied to both time- and frequency-domain wheel/track interaction modelling ([10], [16], [17]). Regardless of the linearization step, Hertzian theory is based on three assumptions: smooth surfaces, elliptic contact area and the assumption that one line of combined roughness represents the three-dimensional roughness profile within the contact area of 0.8 to 2.5 cm^2 [17]. In practice, short roughness wavelengths smaller than the contact dimensions should be filtered in order to achieve realistic predictions in the high frequency range and the correlation of the roughness profile in the longitudinal and lateral direction influences the level of excitation [18].

Over the years, methods to increase the accuracy of the effective combined roughness profile have been developed, such as two- and three-dimensional elastic foundation models [2]. These models rely on a pre-calculation of the (non-linear) contact stiffness and the effective combined roughness profile and solve the wheel/track interaction problem as a point contact problem. In [18] detailed three-dimensional contact modelling is included in the time-domain wheel/track dynamic interaction model, eliminating all simplifications related to the point contact assumption.

Although time-domain models of wheel-track interaction including three-dimensional contact modelling enable predictions of high accuracy, they entail a high computational cost and require complete three-dimensional roughness data for the total length along the rolling direction. Therefore in [19] a method is proposed that captures the roughness- and shape-induced non-linear effects on both contact stiffness and contact filtering, while keeping the single-point contact approach, leading to a low computational cost and a limited amount of input roughness data. This method is a further development of the contact model developed and validated in [20] for the general case of steel-steel rolling contacts.

The resulting state-dependent nonlinear contact stiffness is plotted in Figure 5 for a low and a high roughness profile, together with the Hertzian contact stiffness for comparison [19]. Figure 5 clearly shows that the larger the amplitude of the combined roughness

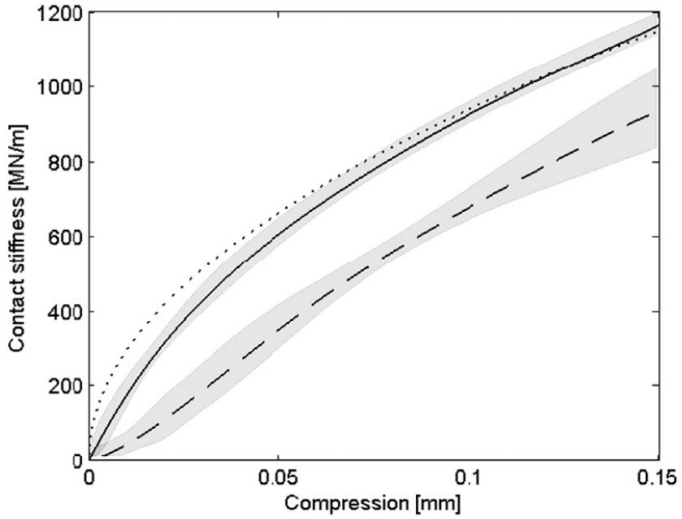

Figure 5: Contact stiffness for low roughness contact (solid) and high roughness contact (dashed), with two standard deviations above and below the curve-fitted values (shaded), Hertzian contact stiffness as defined in ([16]) (dotted).

profile the more the contact stiffness deviates from the Hertzian contact stiffness. For the same compression, an increase of the surface roughness amplitude leads to a smaller area of real contact and, therefore, a smaller contact force and a contact stiffness significantly lower than the Hertzian contact stiffness.

During rolling the contact area changes due to dynamic load variations and so does the spatial filtering, which implies that the spatial filtering is nonlinear with respect to the vertical compression. In Figure 6 the filter effect for the two combined roughness profiles considered and several static load values is shown. Details about the method used to derive these filters can be found in [19]. It can be seen that the contact filter spectra display dips at frequencies corresponding to roughness wavelengths which are similar to the length of

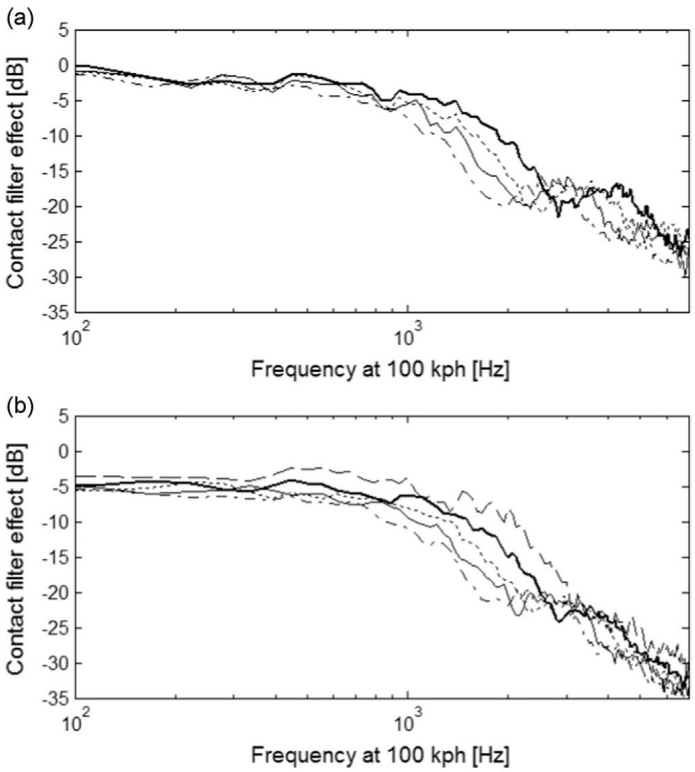

Figure 6: Contact filter effect for static pre-loads 10kN (dashed), 25kN (thick solid), 45kN (dotted), 67.5kN (thin solid) and 100kN (dash-dotted) for (a)low roughness contact and (b) high roughness contact.

the apparent contact area. These dips seem to be more pronounced for the low roughness contact than for the high roughness contact, which is possibly explained by the fact that the contact length for the low roughness profile is well-defined as compared to the high roughness contact, leading to a more Hertzian-like pressure distribution. Furthermore, the high roughness contact leads to a larger contact filtering effect than the low roughness contact. A possible explanation is that, for the high roughness contact, parts of the wheel-rail material within the apparent contact area are not in contact leading to a reduced roughness-excitation. Although the filtering effect increases with increasing frequency (decreasing wavelength), it does not appear to be restricted to wavelengths shorter than (or of the order of) the contact dimensions.

In general it can be concluded that state-dependent contact filtering leads to a larger contact filtering effect than the Hertzian contact model with contact filtering by averaging over the contact length and that the effect is more pronounced for the higher roughness profile. Regarding the comparison between the linear (static) and nonlinear (dynamic) filtering, the largest differences are found for the low static loads and high roughness profile, reaching 8-10 dB for the vehicle speed of 200 kph. The influence of nonlinearities at lower vehicle speeds is however moderate [19].

3.2 Understanding tyre/road rolling contact interaction

The relatively low rigidity of rubber, together with its viscoelastic properties and the higher level of surface roughness of roads compared to metal-metal contacts leads to some fundamental differences in rolling contact conditions. In contrast to a railway wheel

a tyre has the ability to transfer very high longitudinal and transverse forces between vehicle and road and to effectively mitigate the normal contact forces originating from the impact of the tread blocks on the road. This beneficial performance comes at the cost of a higher complexity of the rolling contact interaction. The bending and compression of the tyre when it goes through the contact patch give rise to longitudinal forces on the tread block which in the impact phase act in the tyre rolling direction and in the release phase act in the direction of the vehicle. For perfectly free rolling tyres, these contributions balance each other and lead to a zero net longitudinal force. However, in all real rolling conditions there is always a net longitudinal acceleration or braking present in the tread-block/road contact although it can be low in magnitude if it is present only to overcome the rolling resistance of the vehicle. As shown in Figure 7 the contact forces generated in the rolling process lead to several unwanted effects such as: tyre wear, rolling resistance and noise. Understanding the generation of tyre/road contact forces is the key to a better control of these effects. The vast majority of tyre/road contact interaction models

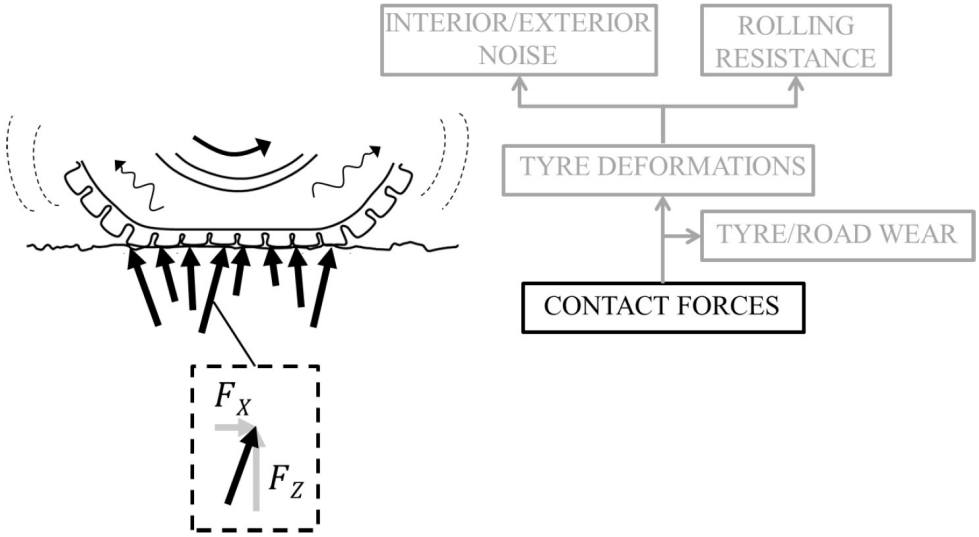

Figure 7: Contact forces in the tyre/road interface generate interior and exterior noise as well as rolling resistance and wear [4].

for vibro-acoustic prediction purposes that can be found in the literature consider only vertical contact forces ([21], [11], [22]) and disregard the longitudinal and transversal (friction) forces. This is partly due to the fact that the rubber/road contact interaction processes that ultimately lead to the friction force are still not fully understood and there is, therefore, a need for empirical data. Although there are several measurement methods that measure contact forces on complete tyres [23], the contact forces are indirectly derived from forces measured in the wheel hub, which is valuable for global validation of tyre models but provides no information on the interaction between tyre-tread and road roughness within the contact. Several works can be found where methods to measure sliding friction between a single tread block and a substrate, excluding the complete tyre structure, are presented (see for example [24] and [25]). However few methods can be found that attempt to measure contact forces between a tread block and a substrate in rolling conditions. In [26] a high speed rolling test rig is developed which is used to measure the normal and longitudinal rolling contact forces between a single tread block and a single stone asperity and more recently a compact internal drum (CID) measurement

set-up is proposed, where the interaction between a tread block and an asphalt substrate is studied for representative impact and release conditions [27].

The compact internal drum (CID) test rig (see Figure 8) is developed for measurements of the three contact force components generated in the impact and release phase of a tyre tread block in rolling contact with a substrate. The design of the test rig is such that realistic impact and release angles for the tread block–substrate contact are provided and force measurements at high rolling speeds with a high signal-to-noise ratio are enabled. It is suitable for detailed investigations of the influence of rubber tread block and substrate characteristics on the contact forces, since both the substrate as well as the sample tread block are fully interchangeable.

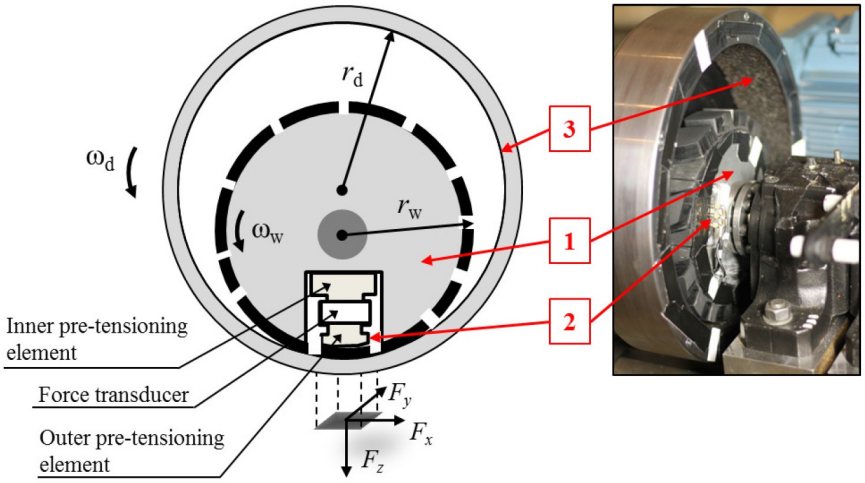

Figure 8: The core of the test rig consists of a solid metal wheel (1) within which a force link (2) including a tread block sample is embedded. In test rig operation, the solid metal wheel rolls on the inner surface of a drum (3), which is covered by an interchangeable sample substrate [27]

The vertical compression of rubber leads to vertical compressive stresses as well as longitudinal shear stresses directed towards the center of the contact area. A sinusoidal-like longitudinal force history is found since the tread block is deformed towards the leading edge at impact and subsequently deformed towards the trailing edge in the release phase. In Figure 9(a), this sinusoidal-like character is distorted by a superimposed shear force directed towards the leading edge which correspond to the force required to overcome the rolling losses of the test rig and maintain a constant velocity. The force history immediately after the driving torque has been removed is presented in Figure 9(b), where the superimposed longitudinal shear force is directed towards the trailing edge. This sinusoidal-shaped force history is found in numerous experimental investigations of the longitudinal forces on complete rolling tyres (see for example [28]) as well as in the investigation of a single tread block in rolling contact performed by [26]. Due to the asymmetry of the tread block shape (leading and trailing edge are not perpendicular to the direction of travel), also a transverse shear force is measured, although it is small compared to both the vertical and the longitudinal force components.

Constant acceleration is simulated by the application of a braking torque to the drum and simultaneously a driving torque generated by the electric motor sufficient to maintain a constant rolling velocity. In Figure 9(c)-(d), the resulting contact forces are presented for simulated constant acceleration at the rolling velocity 3.6 m/s. In this case, as one would

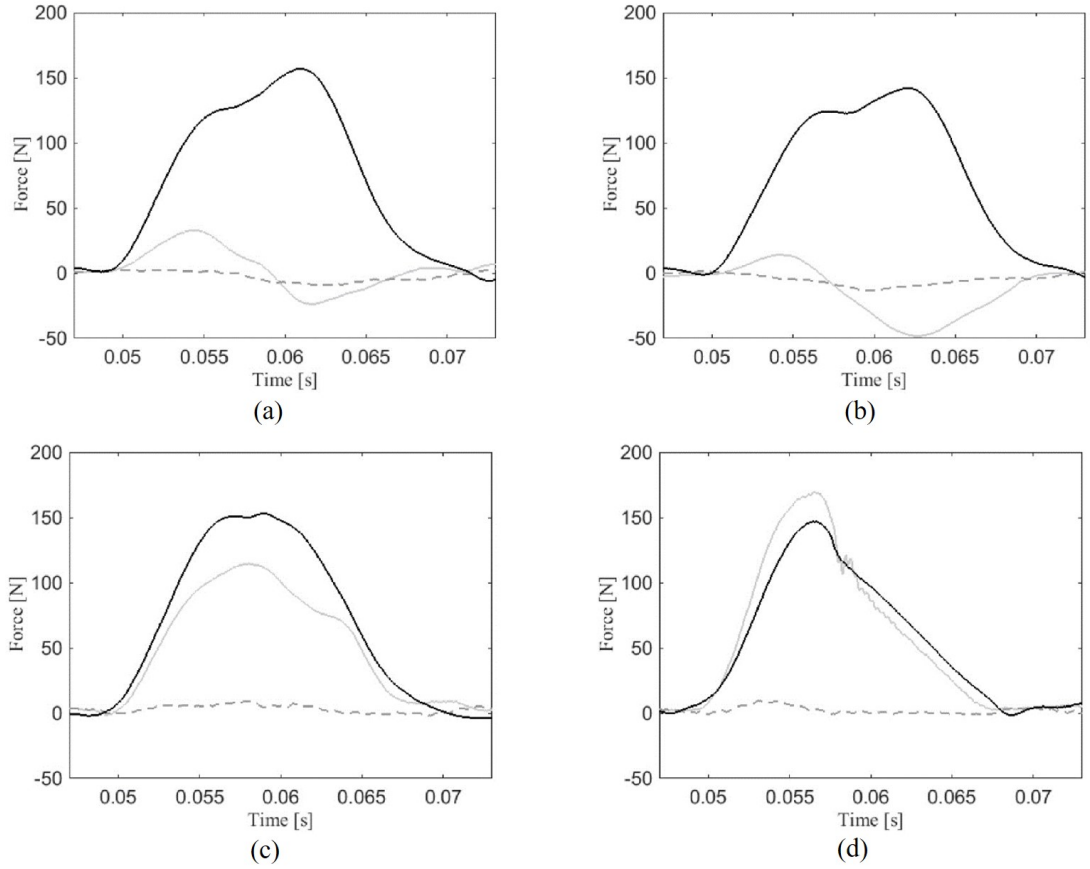

Figure 9: Measured longitudinal (solid grey), transverse (dashed) and vertical (solid black) contact forces for rolling velocity 3.6 m/s and static load 70 N; (a) with driving torque; (b) without driving torque; (c) with driving torque and braked drum (sx = 0:038); (d) with driving torque and heavily braked drum (sx = 0:100). NCC Repasfalt / Vialit Reaktiv Asphalt, maximum stone size 4mm [27].

expect, the longitudinal force is positive for the complete contact length and significantly larger than before. For the heavy breaking conditions the longitudinal force is larger than the normal force, which leads to a friction coefficient larger than one, which is in agreement with experimental results presented by [29].

In order to explore how the rolling conditions influence the frequency content of the longitudinal contact force, the average frequency spectrum of the longitudinal forces for the four surfaces considered it displayed in Fig. 10 in free-rolling and heavy acceleration conditions.

At the velocity of 62 km/h and approximate free rolling condition, the frequency content of the longitudinal force presented in Fig. 10 is seen to be fairly similar for the two asphalt surfaces. In contrast, the corresponding results for heavy acceleration, which are believed to induce slip and stick–slip condition in the trailing half of the contact length reveal large differences above approximately 400 Hz. Although a broadband increase is found for both cases which is prominent for the approximate frequencies of 800 and 2700 Hz, it is much larger for the results corresponding to the asphalt with 11mm stone size than for that with 4mm stone size, which supports the previous observation concerning a more considerable onset of slip for the asphalt with 11mm stone size. Even larger differences of the frequency content are found for the results corresponding to

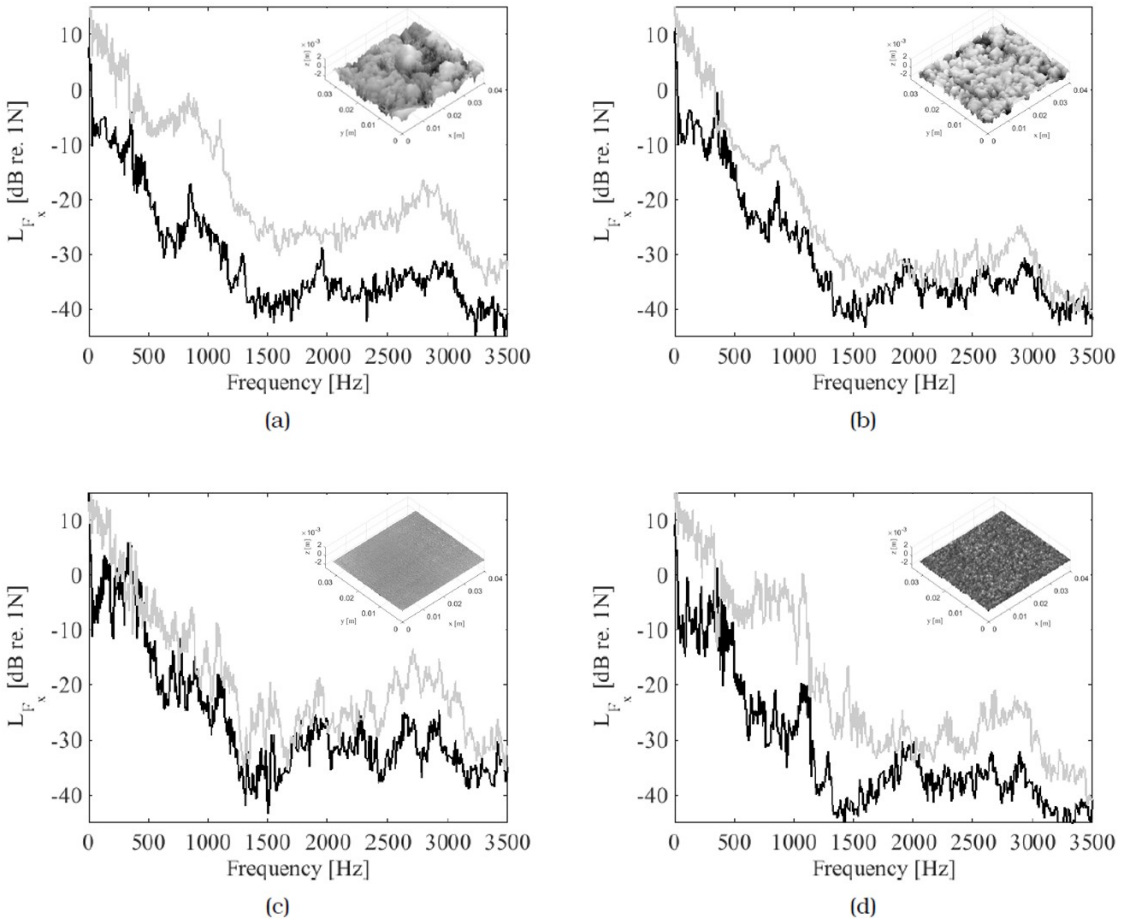

Figure 10: Averaged linear spectra of the longitudinal force (rms) as a function of frequency for approximate free rolling (black) and heavy acceleration (grey) at 62 km/h; a) asphalt with stone size 11 mm; b) asphalt with stone size 4 mm; c) aluminium substrate; d) anti-slip tape substrate [4, 30].

the aluminium substrate and the anti-slip tape substrate. For the aluminium substrate, a generally higher and broadband level is exhibited for the free rolling condition compared to all the other substrates which is for the case of heavy acceleration intensified mainly around the approximate frequency of 2700 Hz. The results for the anti-slip tape substrate reveal a more moderate broadband contribution for the approximate free rolling condition, whereas a drastically increased contribution is found for the heavy acceleration case although the increase is most prominent around the frequencies of 800 and 2700 Hz. Conclusively, the observations presented here regarding the frequency content of the longitudinal force component may have considerable importance for the understanding of the influence of substrate roughness on friction induced tread wear and noise generation.

The capability of the test rig to generate useful results is assessed by presenting results for both free rolling and accelerating condition at different rolling velocities and different static vertical pre-loads. The test rig thus provides results which contribute to the understanding of tyre/road interaction and can be used as input to modelling-based development of both tyres and roads aiming for improved handling, safety, energy efficiency, comfort and acoustic performance.

4. SEPARATION OF RAILWAY ROLLING NOISE SOURCES

4.1 Background

In railway pass-by noise, rolling noise dominates for trains travelling at speeds below 300 km/h [31]. With the aim of legal homologation, the technical specification for interoperability (TSI) NOISE regulates the sound levels of European rail-bound vehicles to specific limit values [32]. It has however been found that a significant part of the pass-by noise comes from the track at frequencies below 2 kHz, and for this reason the compliance of a vehicle with the TSI legislation nowadays largely depends on the track on which such a vehicle runs. Therefore the need for separating the track and vehicle contributions to the meassured pass-by noise arises in order to facilitate the homologation process.

Over the years, several separation techniques have been proposed. The MISO (Multiple Input Single Output) method obtains an estimate of the rail contribution by means of measured rail vibration spectra and a transfer-matrix, and the wheel contribution is inferred from the level difference between the total pass-by and the rail contribution [33] .The VTN (Vibro-acoustic Track Noise) method proposed in [34], estimates the sound levels using source models from TWINS [35] for measured vertical and lateral rail vibrations and sleeper vibrations. The method currently in use is the PBA (Pass-by Analysis) technique [36], which is a transfer-matrix method that can separate the contributions down to roughness levels, by means of knowledge of rail vibrations and sound pressure at one microphone located as defined in ISO3095 [37]. Other separation techniques include the use of one- and two-dimensional microphone arrays [38, 39, 40], beamforming arrays. However, a common drawback of beamforming is that it underestimates the rail contribution by at least 10 dB. The cause of this underestimation is that beamforming arrays are most suitable for uncorrelated sources, which is not the case for a spatially extended source such as the rail. The most recent alternative to beamforming is the so-called SWEAM (Structural Wavenumbers Estimation with an Array of Microphones) method [41], which calculates an inverse estimation of the structural wavenumbers and decay rates of the waves in the rail.

In the Horizon2020 Shift2Rail project Roll2Rail a number of existing and newly proposed methods have been tested and compared [42]: PBA, MISO, TWINS with measured track vibration, beamforming, advanced transfer path analysis (ATPA) and wave signature extraction (WSE). The latter method is presented in the next section, where a short description of the method is provided and the main results are sumarized. A detailed description of the WSE method can be found in [43].

4.2 Wave Signature Extraction (WSE)

4.2.1 Brief description of WSE

A railway track consists of the rails, pads, sleepers, and ballast. The sound radiation of the sleepers dominates up to 500 Hz, specially for a track with stiff pads [44]. Below this frequency, the rail often behaves like a compact source, and most of the sound radiation is concentrated in a small region close to the contact point with the wheel. As the frequency increases, the structural waves begin to propagate freely in the rail, and the latter behaves like a distributed source. Then the rail sound radiation becomes dominant up to about 1600 Hz. Above this frequency it is frequently the case that the rail noise is surpassed by the wheel noise. In the frequency range in which the rail behaves like an extended

source, the sound field consists of plane waves propagating at an angle to the normal of the rail longitudinal axis. This radiation angle, lying in the $x-z$ plane, is characterized by the ratio of the acoustic wavelength and the wavelength of the bending wave that is excited in the rail. Fig. 11 shows a schematic of this situation, in which the angle follows $\phi = \arcsin(\lambda/\lambda_B) = \arcsin(k_B/\kappa)$, where k_B and κ are the bending and acoustic wavenumbers respectively.

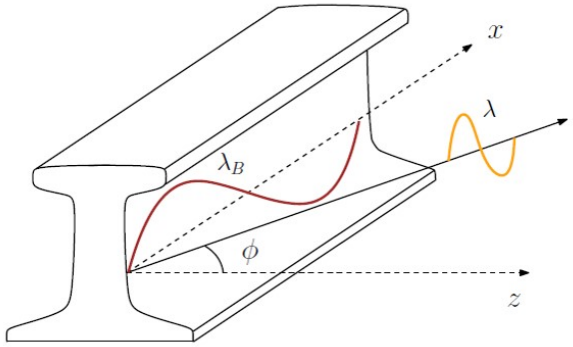

Figure 11: Sound radiation directivity of the rail. Plane waves are radiated at an angle ϕ in the $x-z$ plane, and λ and λ_B are the wavelengths of the acoustic and structural waves [43].

During a train pass-by, the rail radiation has contributions from vertical and lateral bending waves. In general, lateral waves cut-on earlier in frequency than vertical waves because of a difference in stiffness, and there can be a total of at least four wave families up to 5 kHz [45]. In order to distinguish between plane–wave families it is convenient to represent the fields in a dispersion plot. This is a plot of the wave amplitude versus wavenumber κ and frequency f. Fig. 12 illustrates the dispersion plot obtained from a vertically excited Timoshenko beam model, and the calculated dispersion from two bogies passing in front of a microphone array. It can be seen that the dispersion

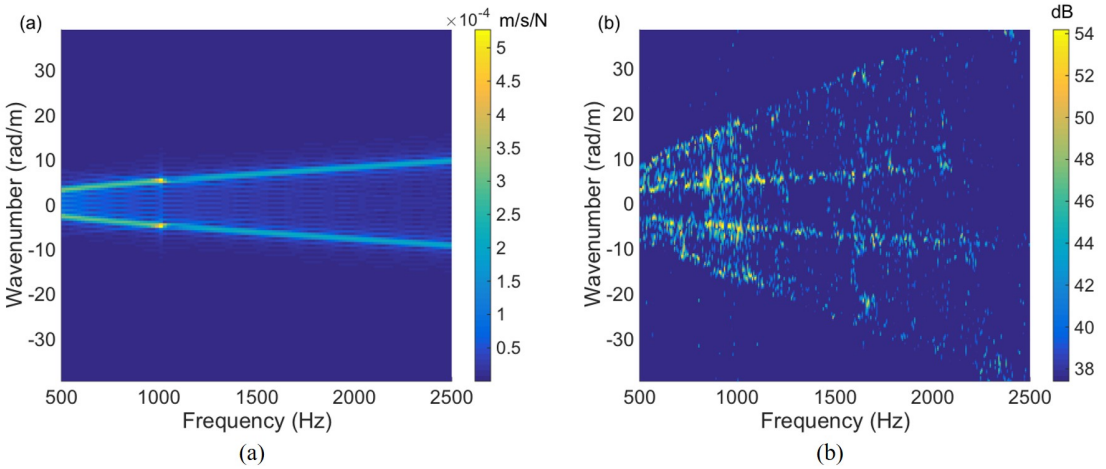

Figure 12: Dispersion plot signatures obtained from (a) vertical mobility of a periodically supported Timoshenko beam model, and from (b) array pressure measurements for a train pass-by section corresponding to two bogies running at 160 km/h [43].

behavior observed in the acceleration data (Fig. 12(a)) is also found in the array pressure measurement data (Fig. 12(b)), as expected from earlier measurements on an epty track

[44]. Additionally, waves that possibly correspond to noise radiated by the wheels and the sleepers are identified.

The main principle of the WSE method is to separate the rail noise by means of filtering the wavenumber spectra obtained from microphone array measurements of the train pass-by. The key point is the design and application of the wavenumber filters according to the rail signature measured with the microphone array. As mentioned above, the rail signature consists of plane waves that typically can be represented as narrow–band signals in the wavenumber domain, hence justifying the application of band-pass wavenumber filters that only accept the narrow–band content and reject the rest of the spectrum.

In general the rail signature can be estimated given the knowledge of the structural properties of the track, which would usually require a static test besides the actual train pass-by measurement. In this work, however, the rail signature is estimated from pressure and acceleration recordings taken a few seconds before and after the pass-by event, provided the microphone array is located in the near-field of the rail and two accelerometers are located on the rail: one in the vertical and one in the lateral direction. This procedure to estimate the rail signature allows for the design of the band-pass wavenumber filters without the need of the additional static measurement. An overview of the signal processing chain from time–domain signals to the rail sound pressure levels is shown in Fig. 13.

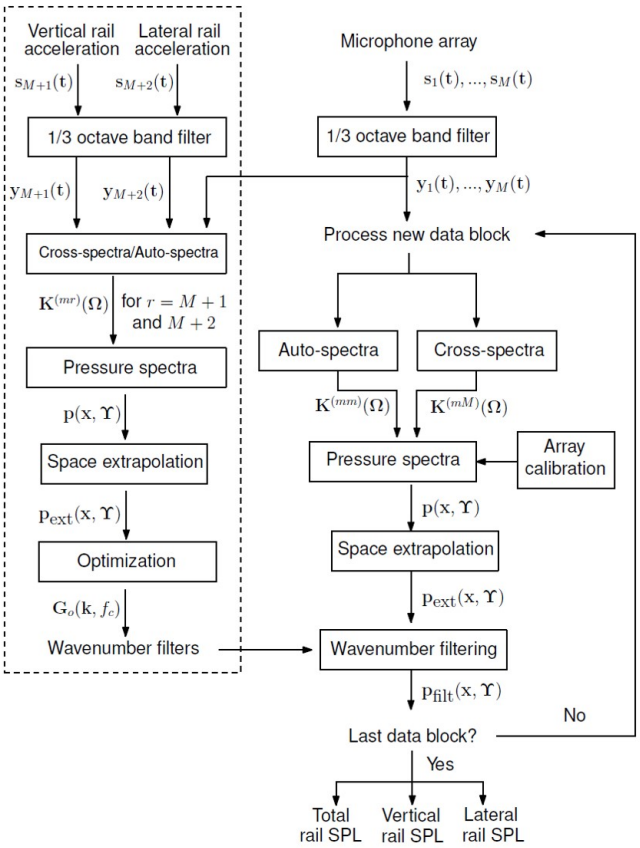

Figure 13: Block diagram of the wave signature extraction method. The dashed box comprises the estimation of the optimal filter with data before and after the train pass-by [43].

The processing steps within the dashed box on the left of Fig. 13 correspond to the identification of the filter parameters based on the microphone signals just before and

just after the train pass-by. The vertical and lateral acceleration signals are used as a reference to improve the quality of the pressure spectra used for the filter estimation. The steps on the right column (outside the dashed box) correspond to the preprocessing and consequent filtering of the microphone array data. As a result the rail contribution in 1/3 octave bands is obtained, as well as the vertical and lateral vibration contributions. A detailed explanation of each of the signals and processing blocks involved in the WSE method can be found in [43].

4.2.2 Experimental results

The measurement campaign was carried out in a high-speed track with standard ballast, near Munich, Germany, in June 2016. The experimental setup is shown in Figs. 14.

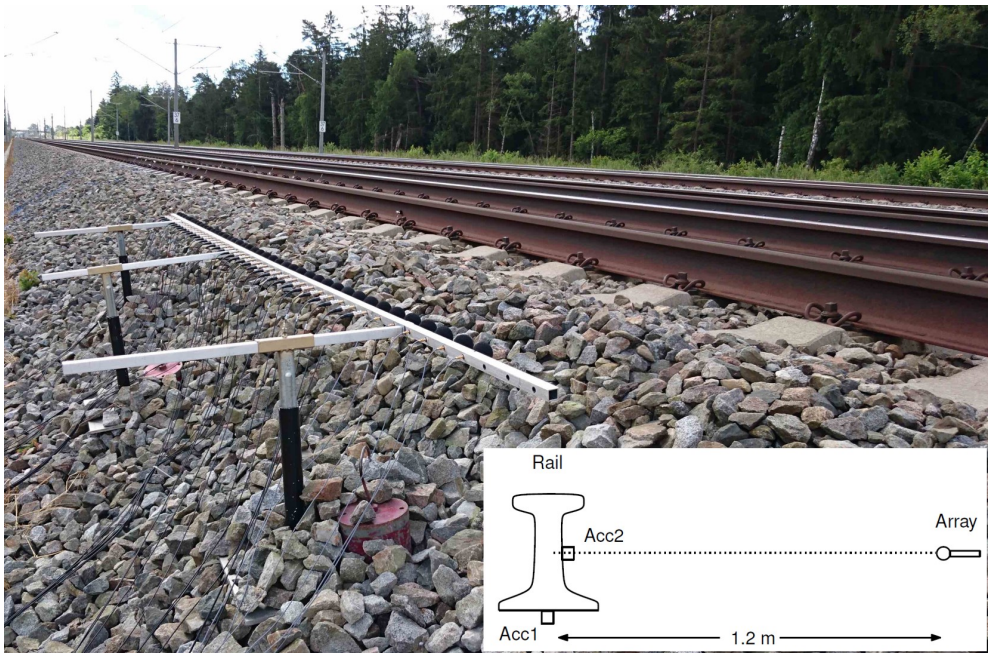

Figure 14: Photograph and schematic side-view of the pass-by measurement setting in Germany [43].

It consists of a 42-channel line microphone array, two accelerometers and a pass-by microphone located 7.5 m away from the track center as defined in ISO3095 [37]. The array consists of 6 GRAS 40BD and 36 GRAS 40PH microphones. The acceleration sensors are ICP accelerometers B&K 4398, and the pass-by microphone is a BSWA Tech MA201. All sensors are connected to a VXI multi-channel acquisition system, and the time signals are simultaneously sampled at 6.4 kHz. The microphone array is positioned 1.2 m away from the nearest rail, and at half the rail web in height. The array is held on an aluminium frame, which rests on three supports fixed with ballast. The microphone spacing is 8 cm, which gives an array length of 3.36 m. Windshields are used in order to minimize the influence of flow in the measurements. The accelerometers are mounted with magnets vertically underneath the rail and laterally at half the rail web, and located in front of the left-most microphone of the array. Two train passages at 80 km/h and at 160 km/h are considered. The corresponding rail contributions to the sound pressure level spectra predicted by WSE are given in Fig. 15, along with the TWINS predictions.

Firstly it can be stated that the rail sound pressure level spectra are very close to the total pass-by spectra for both travelling velocities, thus there is a significant contribution

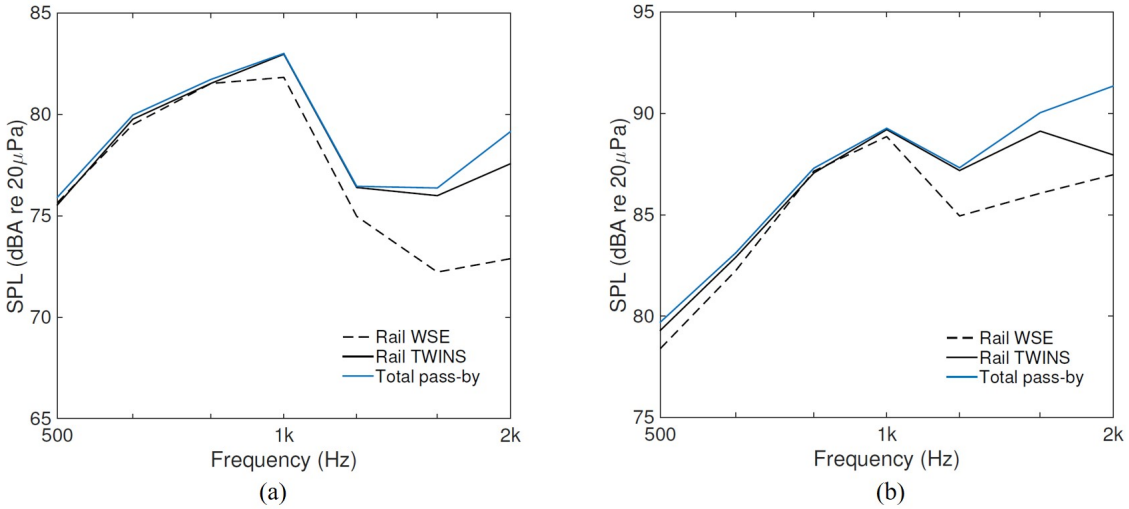

Figure 15: Sound pressure level spectra of the rail contribution for the train running, predicted by TWINS and the WSE method. The total pass-by is that predicted by TWINS. (a) 80 km/h, (b) 160 km/h [43].

from the rail in the measured pressure in this frequency range. Overall the rail contribution obtained with the WSE method agrees well with the predictions from TWINS. However, an underestimation of the rail contribution by the WSE method can be seen at 1600 and 2000 Hz. A closer study of the rail dispersion characteristics measured in [43] indicates that this underestimation might be due to the appearance of the next bending wave families, with cut-on frequencies of about 1500 Hz. These wave are filtered out by the filters designed in [43], which only consider the first vertical and lateral bending wave families. The possibility of including additional bending wave families is studied in [46], where the filters schematically drawn in Fig. 16 are designed and assessed for their effectiveness.

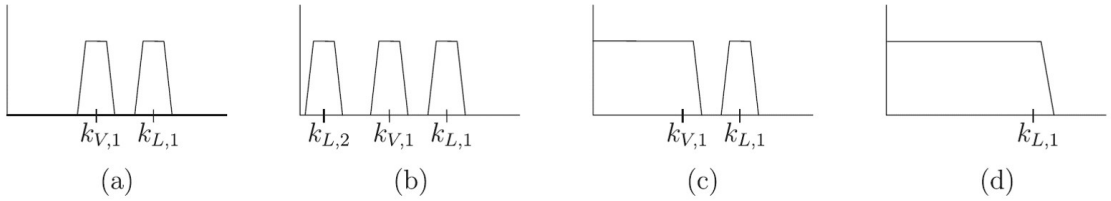

Source: Zea et al., 2018

Figure 16: Wavenumber–domain filter functions investigated: (a) scheme I: double bandpass [43], (b) scheme II: triple bandpass, (c) scheme III: low and bandpass, and (d) scheme IV: low-pass.

Four different filtering schemes are proposed in Fig. 16, starting with the filtering scheme from [43] (scheme I). The remining filtering schemes: II to IV consider different ways of including a broader range of frequencies. In Fig. 17 a table with the sound pressure level values at 3rd-octave bands 1600Hz and 2000 Hz, obtained for the different filtering schemes is provided, along with the TWINS prediction. The closest estimates are boldfaced.

For 1.6 kHz and both train speeds, the use of triple bandpass filters (scheme II) appears to reduce the underestimation obtained with the original WSE filters (scheme I) by about

Speed (kph)	f_c (Hz)	TWINS (dBA)	I[a] (dBA)	II (dBA)	III (dBA)	IV (dBA)
80	1600	76.00	72.23	**75.21**	74.27	72.36
	2000	77.57	72.89	75.82	**75.89**	73.79
160	1600	89.12	86.06	**88.91**	88.86	87.16
	2000	87.95	86.97	89.64	89.38	**87.23**

Source: Zea et al., 2018

Figure 17: Rail contributions via filtering schemes I–IV, against reference data predicted by TWINS ([a] reference [43].

3 dB. At 2 kHz and 80 kph train speed, the SPL obtained via filtering scheme III is closest to that predicted by TWINS, although scheme II is rather close as well—just 0.07 dB difference from scheme III. Last, at 2 kHz and 160 kph speed, scheme IV gives the closest estimate to TWINS' predicted value, while schemes II and III overestimate the rail contribution by about 1.5 dB. All in all, the triple bandpass filter (scheme II) seems to provide the best overall estimation, supporting the expectation that including higher order bending waves would improve the estimation.

4.2.3 Discussion

Although the implementation of the WSE method presented here makes use of a uniform line microphone array and two accelerometers, it is straightforward to extended it to two-dimensional microphone arrays . The novelty of this work lies in the introduction and application of rail wavenumber filters to microphone array measurements of the train pass-by. In its current form, the method is limited to the frequency range in which the rail behaves like a distributed source. The advantage of the method is that no prior knowledge of the structural properties of the track is in principle needed. This means no additional measurements are needed, reducing the track-acces time required. However, the track choosen for the measurement campaign in Germany is a soft track with relatively high decay rates. It remains to be seen whether this conclusion will hold for a stiff track as well, since the available pre- and post-passby signal might be too short to allow an accurate estimation of the dispersion properties of the rail. The comparison to TWINS demonstrates that the WSE method predicts well the total rail contribution, except at the frequencies at which the wheel contribution dominates the pass-by noise. Nevertheless there is room for application of the method even at frequencies in which the wheel is dominating (above 2kHz), by means of using a denser microphone array. At these frequencies care must then be taken of possible discrepancies of the rail signature with and without the train on the track.

5. CONCLUSIONS

This paper discusses the similarities and differences in the sound generation process of rolling noise for road and rail vehicles. It is shown that in essence the force and vibration generation mechanisms are similar and the both problems can be modelled following analogous approaches. Nevertheless, the specific contact interaction conditions and the sound radiation mechanisms are very different. These two aspects are discussed in this paper. Since the key to minimizing rolling noise generation are the contact forces, this paper further explores rolling contact interaction from the modelling perspective for

wheel/rail interaction and from the experimental perspective for tyre/road noise. Finally, the issue of railway rolling noise source separation is addressed and methods to establish the track contribution to the total pass-by noise are discussed.

ACKNOWLEDGEMENTS

I would like to thank Oskar Lundberg and Elias Zea for the great work they did during their PhD, parts of which are summarized in this paper. Oskar Lundberg's work was financially supported by the Centre for ECO2 Vehicle Design, while Elias Zea's work received financial support from H2020 Shift2Rail project Roll2Rail (grant agreement No. 636032) and the Swedish Research Council (grant agreements No. 2012-3723 and No. 2015-04258).

6. REFERENCES

[1] Ulf Sandberg and Jerzy A Ejsmont. *Tyre/road noise reference book*. Informex, SE-59040 Kisa, Sweden, 2002.

[2] David Thompson. *Railway noise and vibration: mechanisms, modelling and means of control*. Elsevier, 2008.

[3] Ines Lopez Arteaga. Vibro-acoustic sources in ground transportation. In *ACOUSTICS 2017 Perth: Sound, Science and Society-2017 Annual Conference of the Australian Acoustical Society, AAS 2017*. Australian Acoustical Society, NSW Division, 2010, 2017.

[4] Oskar E. Lundberg. On the influence of surface roughness on rolling contact forces.

[5] Ard Kuijpers. Towards silent tracks and roads: beating the roughness. *Proc. ForumAcusticum Budapest*, pages 1159–1164, 2005.

[6] Astrid Pieringer, Luis Baeza, and Wolfgang Kropp. Modelling of railway curve squeal including effects of wheel rotation. In *Noise and Vibration Mitigation for Rail Transportation Systems*, pages 417–424. Springer, 2015.

[7] I. Lopez, R. Blom, N. Roozen, and H.Nijmeijer. *Modelling vibrations on deformed rolling tyres - a modal approach*. *Journal of Sound and Vibration*, 307(3-5):481–494, 2007.

[8] I. Lopez-Arteaga. *Green's functions for a loaded rolling tyre*. *International Journal of Solids and Structures*, 48(25-26):3462 – 3470, 2011.

[9] Luis Baeza, Juan Giner-Navarro, David J Thompson, and Juan Monterde. Eulerian models of the rotating flexible wheelset for high frequency railway dynamics. *Journal of Sound and Vibration*, 2019.

[10] Anders Nordborg. Wheel/rail noise generation due to nonlinear effects and parametric excitation. *The Journal of the Acoustical Society of America*, 111(4):1772–1781, 2002.

[11] DJ O'Boy and AP Dowling. Tyre/road interaction noise—numerical noise prediction of a patterned tyre on a rough road surface. *Journal of Sound and Vibration*, 323(1):270–291, 2009.

[12] Paul J Remington. Wheel/rail rolling noise, i: Theoretical analysis. *The Journal of the Acoustical Society of America*, 81(6):1805–1823, 1987.

[13] K Larsson and W Kropp. A high-frequency three-dimensional tyre model based on two coupled elastic layers. *Journal of sound and vibration*, 253(4):889–908, 2002.

[14] RJ Pinnington. A wave model of a circular tyre. part 1: belt modelling. *Journal of Sound and Vibration*, 290(1):101–132, 2006.

[15] Carl-Magnus Nilsson. *Waveguide finite elements applied on a car tyre*. PhD thesis, Farkost och flyg, 2004.

[16] TX Wu and DJ Thompson. Theoretical investigation of wheel/rail non-linear interaction due to roughness excitation. *Vehicle System Dynamics*, 34(4):261–282, 2000.

[17] Paul J Remington. Wheel/rail noise—part iv: Rolling noise. *Journal of Sound and Vibration*, 46(3):419–436, 1976.

[18] A. Pieringer, W. Kropp, and D.J. Thompson. Investigation of the dynamic contact filter effect in vertical wheel/rail interaction using a 2d and a 3d non-hertzian contact model. *Wear*, 271(1):328 – 338, 2011. Proceedings of the 8th International Conference on Contact Mechanics and Wear of Rail / Wheel Systems, Florence, 2009.

[19] Oskar E Lundberg, Anders Nordborg, and Ines Lopez Arteaga. The influence of surface roughness on the contact stiffness and the contact filter effect in nonlinear wheel–track interaction. *Journal of Sound and Vibration*, 366:429–446, 2016.

[20] Oskar E Lundberg, Svante Finnveden, Stefan Björklund, Mikael Pärssinen, and Ines Lopez Arteaga. A nonlinear state-dependent model for vibrations excited by roughness in rolling contacts. *Journal of Sound and Vibration*, 345:197–213, 2015.

[21] Stijn Boere, Ines Lopez Arteaga, Ard Kuijpers, and Henk Nijmeijer. Tyre/road interaction model for the prediction of road texture influence on rolling resistance. *International Journal of Vehicle Design*, 65(2-3):202–221, 2014.

[22] Julia Winroth, PBU Andersson, and Wolfgang Kropp. Importance of tread inertia and damping on the tyre/road contact stiffness. *Journal of Sound and Vibration*, 333(21):5378–5385, 2014.

[23] H Pacejka. *Tire and Vehicle Dynamics*. Elsevier Ltd,, 2012.

[24] R Van Der Steen, Ines Lopez, and Henk Nijmeijer. Experimental and numerical study of friction and stiffness characteristics of small rolling tires. *Tire Science and Technology*, 39(1):5–19, 2011.

[25] Marko Rantonen, Ari Juhani Tuononen, and Panu Sainio. Measuring stud and rubber friction on ice under laboratory conditions. *International Journal of Vehicle Systems Modelling and Testing*, 7(2):194–207, 2012.

[26] F Liu, MPF Sutcliffe, and WR Graham. Prediction of tread block forces for a free-rolling tyre in contact with a rough road. *Wear*, 282:1–11, 2012.

[27] Oskar E Lundberg, Leif Kari, and Ines Lopez Arteaga. A compact internal drum test rig for measurements of rolling contact forces between a single tread block and a substrate. *Measurement*, 103:370–378, 2017.

[28] R Van Der Steen, I Lopez, H Nijmeijer, A Schmeitz, and B De Bruijn. Experimental and numerical study of friction and braking characteristics of rolling tires. *Tire Science and Technology*, 39(2):62–78, 2011.

[29] R Van der Steen. *Enhanced friction modeling for steady-state rolling tires*. PhD thesis, 2010.

[30] Oskar E Lundberg, Leif Kari, and Ines Lopez Arteaga. An experimental study on the influence of substrate roughness on the friction of a tread block in rolling and sliding contact. *Submitted*, 2019.

[31] P.-E. Gautier, F. Poisson, and F. Letourneaux. High Speed Trains external noise: a review of measurements and source models for the TGV case up to 360km/h. In *World Congress Railway Research*, pages 1–10, Seoul, 2008.

[32] Commission Regulation (EU) No 1304/2014 of 26 November 2014 on the technical specification for interoperability relating to the subsytem 'rolling stock – noise' amending Decision 2008/232/EC and repealing Decision 2011/229/EU Text with EEA relevance, 2014.

[33] Fabien Letourneaux, Olivier Coste, Cyril Mellet, and Pascal Fodiman. Environmental Railway Noise: a Source Separation Measurement Method for Noise Emissions of Vehicles and Track. In *Forum Acusticum*, pages 1–6, Sevilla, 2002.

[34] Edwin Verheijen and Marco Paviotti. VTN: A validated method to separate track and vehicle noise and to assess noise reduction measures. In *World Congress Railway Research*, pages 1–9, Edinburgh, 2003.

[35] David Thompson. Sound Radiation from Wheels and Track. In *Railway Noise and Vibration*, chapter 6, pages 175–222. Elsevier, Oxford, 2009.

[36] M.H.A. Janssens, M.G. Dittrich, F.G. de Beer, and C.J.C. Jones. Railway noise measurement method for pass-by noise, total effective roughness, transfer functions and track spatial decay. *Journal of Sound and Vibration*, 293(3-5):1007–1028, jun 2006.

[37] ISO 3095 Acoustics - Railway applications - Measurement of noise emitted by railbound vehicles, 2013.

[38] T. Kitagawa and D.J. Thompson. Comparison of wheel/rail noise radiation on Japanese railways using the TWINS model and microphone array measurements. *Journal of Sound and Vibration*, 293(3-5):496–509, jun 2006.

[39] T. Kitagawa and D.J. Thompson. The horizontal directivity of noise radiated by a rail and implications for the use of microphone arrays. *Journal of Sound and Vibration*, 329(2):202–220, jan 2010.

[40] F. Le Courtois, J.-H. Thomas, F. Poisson, and J.-C. Pascal. Identification of the rail radiation using beamforming and a 2 D array. In *Acoustics*, pages 3745–3750, Nantes, 2012.

[41] Baldrik Faure, Olivier Chiello, Marie-Agnès Pallas, and Christine Servière. Characterisation of the acoustic field radiated by a rail with a microphone array: The SWEAM method. *Journal of Sound and Vibration*, 346:165–190, jun 2015.

[42] David Thompson, Giacomo Squicciarini, Jin Zhang, Ines Lopez Arteaga, Elias Zea, Michael Dittrich, Erwin Jansen, Kevin Arcas, Ester Cierco, Francesc Xavier Magrans, et al. Assessment of measurement-based methods for separating wheel and track contributions to railway rolling noise. *Applied Acoustics*, 140:48–62, 2018.

[43] E Zea, L Manzari, G Squicciarini, L Feng, DJ Thompson, and Ines Lopez Arteaga. Wavenumber-domain separation of rail contribution to pass-by noise. *Journal of Sound and Vibration*, 409:24–42, 2017.

[44] Elias Zea, Luca Manzari, Ines Lopez Arteaga, Giacomo Squicciarini, and D.J. Thompson. Separation of track contribution to pass-by noise by near-field array techniques. In *22nd International Congress on Acoustics*, pages 1–10, Buenos Aires, 2016.

[45] D.J. Thompson. Experimental analysis of wave propagation in railway tracks. *Journal of Sound and Vibration*, 203(5):867–888, jun 1997.

[46] E Zea and Ines Lopez Arteaga. On modifed wavenumber filters for rail contribution estimations. *Journal of the Acoustical Society of America*, 144(4):EL286–EL289, 2018.